



Analytical Investigation of Flow of a Micropolar Fluid Between Disks with Vertical Magnetic Field

Reshu Gupta¹

Accepted: 20 December 2023 / Published online: 1 April 2024

© The Author(s), under exclusive licence to Springer Nature India Private Limited 2024

Abstract

Analytical investigation is held on the steady and axisymmetric flow model in a porous medium containing a micropolar fluid between two disks. Using the proper similarity transformation, the system of velocity and microrotation partial differential equations is transformed into a non-dimensional form. The differential transform technique, which produces an output in the form of a series, is used to determine the estimated solution to these equations. On this spot, there is a detailed discussion and visual representation of how the micropolar parameter, Reynolds number, and magnetic field parameter affect the velocity and microrotation profiles. The numerical values of couple stress and the skin friction are compared to data that have already been published. The findings produced by DTM are compared with the data acquired by numerical techniques to verify the method's correctness and validity. It can be found that the behavior of the microrotation profile is very close to the normal graph from the lower to the upper disk. The magnetic field effect will assist in improving the performance of oil extraction drilling systems used in mining industry and the other geothermal applications.

Keywords Differential transform method · Porous disks · Magnetohydrodynamics · Micropolar fluids

Introduction

The flow of fluid between two porous disks has a huge application in industries. This type of flow has been used in the manufacturing of semiconductors, in the engines of gas turbines, storage devices for computers, etc. Researchers have too much interest in this area because of the theoretical and practical importance. Eringen [1] was the first who proposed the basics of micropolar fluids. Such fluids are a subclass of microfluids. The model micropolar fluids are used to define the flow of liquid crystals, flow of blood, flow in capillaries and microchannels, porous medium, etc. Eringen [2] updated his theory of micropolar fluid in the year 1966. Eringen [3] and Lukaszewicz [4] have also discussed micropolar fluid. Rashidi et al. [5] studied nanofluid flow in the model of rotating porous disks. They discussed the effect of

✉ Reshu Gupta
rgupta@ddn.upes.ac.in

¹ University of Petroleum and Energy Studies, Dehradun, UK, India

different physical parameters of the flow and magnetic field. Mahanthes et al. [6] highlighted hydromagnetic nanofluid in their study. They represented the effects of physical constraints by graphs and discussed them in detail. Soid et al. [7] analyzed MHD flow in a stretching and shrinking disk. They adopted the MATLAB software tool for solving equations. They analyzed the impact of the magnetic field parameter and suction parameter on the shear stress. Aziz et al. [8] modelled MHD 3D flow in a rotating disk. They adopted the ND solve mechanism for solving the equations. Agarwal and Mishra [9] presented MHD forced flow and heat transfer in the problem of rotating disks by using HPM. They also compared HPM results with numerical results to prove the accuracy of HPM. Krishna and Chamkha [10] discussed MHD squeezing flow of nanofluid between parallel disks. They adopted Galerkin's optimal homotopy asymptotic method. They examined the consequence of the key parameters and showed them with graphs. Ibrahim [11] chose time-dependent viscous fluid in the study of the rotating disks. He solved the equations numerically by using the finite difference method. Gupta [12] studied flow due to disk rotation. They used the HPM method in their model. Turkyilmazoglu [13] developed the fluid flow and heat transfer in the problem of the rotating disk. Agarwal [14] analyzed flow between parallel disks with uniform porosity. Venerus [15] studied squeeze flow between porous disks. He considered flow in the liquid films. Waqas et al. [16], Asma et al. [17], Devaki et al. [18], Upadhyay [19], and Lin and Ghaffari [20] have also discussed the model of disks in a different manner.

Recently, many researchers devoted their time to researching the micropolar fluid flow property but few of them have discussed the flow of micropolar fluid in rotating disks because of the complexity of obtained differential equations. Agarwal [21] discussed the micropolar fluid in her problem. She analyzed heat mass transfer with flow profile on various parameters. Doh and Muthamilselvan [22], Takhar et al. [23], Sajid et al. [24], Sadiq et al. [25], Mohyud-Din et al. [26], Bhat and Katagi [27, 28], Pasha et al. [29], Gupta [30], Ahmad et al. [31] and Kushal et al. [32–38] used micropolar fluid as a source fluid in their studies.

Mostly, in the above-mentioned research, equations are solved numerically by using different numerical methods. Few of them used the analytical method for solving equations. Here the author used the differential transform method (DTM) to obtain the solution for ODEs. Zhou [39] introduced the theory of DTM on linear and nonlinear equations in the experiment of electric circuits. Usman et al. [40], Keimanesh et al. [41], Hatami and Jing [42], Agarwal [43], Gupta et al. [44], Balazadeh et al. [45], and Gupta and Agarwal [46] applied DTM in their research. Awati et al. [47] applied the homotopy analysis method to get the approximate solution in their model. Agarwal [48], Gupta [49], and Ganji et al. [50] used HAM and HPM to obtain the solution.

The main goal of this research is to examine the MHD flow of a micropolar fluid, which is filled between two disks. The nonlinear partial differential equations are reformed into a system of nonlinear ODEs by suitable transformation. Such obtained ODEs are solved analytically by using the differential transform method. The effect of Reynolds number, micropolar parameter, and magnetic field parameter on flow profile is discussed and presented by graphs. The values of skin friction and couple stress is compared with numerical method results and literature, which are displayed in tabular form. The novelty of the current study is to discuss the magnetic field effect on velocity and microrotation profiles.

Mathematical Formulation

An axisymmetric, laminar, and steady flow of a micropolar fluid, which is filled between two porous disks is considered. Both disks are resting on the plane $z = -d$ and $z = d$ respectively. A micropolar fluid is chosen as an electrically conducting fluid in the presence of a transverse magnetic field, which is applied perpendicularly on the disks. Let u, v, w be the radial, transverse, and axial velocity and N_1, N_2, N_3 be microrotation components in the cylindrical coordinate system as shown in Fig. 1.

The velocity and microrotation profiles are taken as follows [23]:

$$u = u(r, z), v = 0, w = w(r, z)$$

$$N_1 = 0, N_2 = N(r, z), N_3 = 0. \tag{1}$$

The equations of continuity, flow, and microrotation are given by [23]

$$\frac{u}{r} + \frac{\partial u}{\partial r} + \frac{1}{d} \frac{\partial w}{\partial \eta} = 0 \tag{2}$$

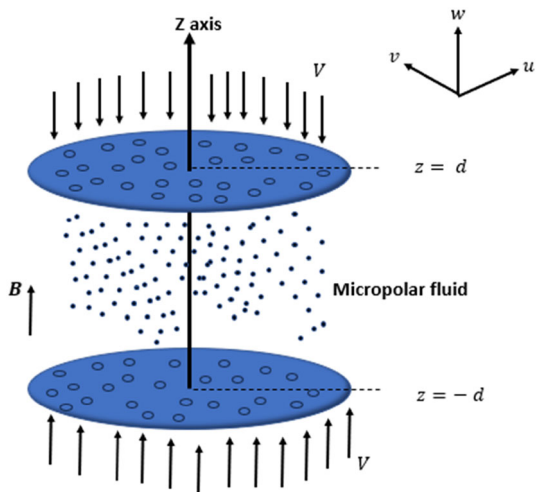
$$\rho \left(u \frac{\partial u}{\partial r} + \frac{w}{d} \frac{\partial u}{\partial \eta} \right) = -\frac{\partial p}{\partial r} - \frac{\kappa}{d} \frac{\partial N}{\partial \eta} + (\mu + \kappa) \left(\frac{\partial^2 u}{\partial r^2} + \frac{1}{r} \frac{\partial u}{\partial r} - \frac{u}{r^2} + \frac{1}{d^2} \frac{\partial^2 u}{\partial \eta^2} \right) - \sigma_e B^2 u \tag{3}$$

$$\rho \left(u \frac{\partial w}{\partial r} + \frac{w}{d} \frac{\partial w}{\partial \eta} \right) = -\frac{1}{d} \frac{\partial p}{\partial \eta} + \kappa \left(\frac{\partial N}{\partial r} + \frac{N}{r} \right) + (\mu + \kappa) \left(\frac{\partial^2 w}{\partial r^2} + \frac{1}{r} \frac{\partial w}{\partial r} + \frac{1}{d^2} \frac{\partial^2 w}{\partial \eta^2} \right) \tag{4}$$

$$\rho j \left(u \frac{\partial N}{\partial r} + \frac{w}{d} \frac{\partial N}{\partial \eta} \right) = \kappa \left(\frac{1}{d} \frac{\partial u}{\partial \eta} - \frac{\partial w}{\partial r} \right) - 2\kappa N + \alpha_1 \left(\frac{\partial^2 N}{\partial r^2} - \frac{N}{r^2} + \frac{1}{r} \frac{\partial N}{\partial r} + \frac{1}{d^2} \frac{\partial^2 N}{\partial \eta^2} \right) \tag{5}$$

where $\eta = \frac{z}{d}$ be the variable of similarity, B be the strength of the magnetic field, ρ is the density of fluid, p be the pressure, j be the micro inertia, μ be the viscosity, κ be the gyro-viscosity, α_1 be the coefficient of gyro-viscosity.

Fig. 1 Flow geometry



The boundary conditions of the problem are as follows:

$$\begin{aligned}
 u(r, 1) = 0, u(r, -1) = 0, w(r, 1) = -V \\
 w(r, -1) = V, N(r, 1) = 0, N(r, -1) = 0
 \end{aligned}
 \tag{6}$$

A stream function defined by [23] is as follows:

$$\Psi(r, \eta) = \frac{V}{2} r^2 f(\eta),
 \tag{7}$$

Therefore $u(r, \eta)$ and $w(r, \eta)$ is defined by

$$u(r, \eta) = \frac{Vr}{2d} f'(\eta)
 \tag{8}$$

$$w(r, \eta) = -Vf(\eta)
 \tag{9}$$

Let

$$N(r, \eta) = \frac{Vr}{2d^2} g(\eta)
 \tag{10}$$

Now substitute the values of u, w, N from Eqs. (8)-(10) into Eqs. (3)-(5). After simplification and eliminating p , we get

$$(1 + R) f^{iv} + R_o f f''' - Rg'' + R_o M_n^2 f'' = 0
 \tag{11}$$

$$\alpha g'' - \beta R_o \left(\frac{1}{2} f' g - f g' \right) + R (f'' - 2g) = 0
 \tag{12}$$

where $M_n \left[= \sqrt{\frac{\sigma_e B^2 d}{\rho V}} \right]$ be magnetic field parameter, $R \left[= \frac{\kappa}{\mu} \right]$ be the micropolar parameter, $R_o \left[= \frac{\rho V d}{\mu} \right]$ be the suction/injection-based Reynolds number, $\alpha \left[= \frac{\alpha_1}{\mu d^2} \right]$, $\beta \left[= \frac{j}{d^2} \right]$ be the micropolar variables.

From Eq. (6), the reduced form of boundary conditions is given by

$$\begin{aligned}
 f(1) = 1, f(-1) = -1, f'(1) = 0, \\
 f'(-1) = 0, g(1) = 0, g(-1) = 0.
 \end{aligned}
 \tag{13}$$

The shear stress and couple stress on the disks is calculated by

$$\tau_{ss} = \left[-(\mu + \kappa) \left(\frac{\partial u}{\partial z} \right) \right]_{z=\pm d} = -\mu(1 + R) \frac{rV}{2d^2} f''(\pm 1)
 \tag{14}$$

$$\tau_{cs} = \left[-\alpha_1 \left(\frac{\partial u}{\partial z} \right) \right]_{z=\pm d} = -\alpha_1 \frac{rV}{2d^3} g'(\pm 1)
 \tag{15}$$

From Eqs. (11), (12) and (13), it is clear that f' is even and g is odd function so that we can say that axial velocity is symmetric along the central line and the microrotation is asymmetric. Therefore, we can consider this model under the region $0 \leq \eta \leq 1$.

So reduced boundary conditions can be written as

$$\begin{aligned}
 f(0) = 0, f(1) = 1, f'(0) = 0, \\
 f'(1) = 0, g(0) = 0, g(1) = 0.
 \end{aligned}
 \tag{16}$$

Methodology of DTM

k Times differentiation of $f(x)$ in this method is given by

$$F(k) = \frac{1}{k!} \left(\frac{d^k f(x)}{dx^k} \right)_{x=x_0} \tag{17}$$

The inverse transformation of $F(k)$ is defined by

$$f(x) = \sum_{k=0}^{\infty} F(k)(x - x_0)^k \tag{18}$$

$f(x)$ can be shown in the form of finite series and hence Eq. (18) can be expressed as

$$f(x) = \sum_{k=0}^n F(k)(x - x_0)^k \tag{19}$$

From Eq. (17) and Eq. (18), we get

$$f(x) = \sum_{k=0}^{\infty} (x - x_0)^k \frac{1}{k!} \left(\frac{d^k f(x)}{dx^k} \right)_{x=x_0}$$

Which represents the Taylor series form of $f(x)$ at $x = x_0$. Following theorems $T_i (i \leq 10)$ can be concluded from Eq. (17) and Eq. (18):

- T_1 : If $f(x) = g(x) \pm h(x)$ then $F(\lambda) = G(\lambda) \pm H(\lambda)$.
- T_2 : If $f(x) = cg(x)$ then $F(\lambda) = cG(\lambda)$, where c is a constant.
- T_3 : If $f(x) = \frac{d^m g(x)}{dx^m}$ then $F(\lambda) = \frac{(\lambda+m)!}{\lambda!} G(\lambda + m)$.
- T_4 : If $f(x) = g(x)h(x)$ then $F(\lambda) = \sum_{\lambda_1=0}^{\lambda} G(\lambda_1)H(\lambda - \lambda_1)$
- T_5 : If $f(x) = e^{ix}$ then $F(\lambda) = \frac{x^\lambda}{\lambda!}$
- T_6 : If $f(x) = x^n$ then $F(\lambda) = \delta(\lambda - n)$ where $\delta(\lambda - n) = \begin{cases} 1, \lambda = n \\ 0, \lambda \neq n \end{cases}$
- T_7 : If $f(x) = g_1(x)g_2(x) \dots \dots \dots g_n(x)$ then

$$F(\lambda) = \sum_{\lambda_{n-1}=0}^{\lambda} \sum_{\lambda_{n-2}=0}^{\lambda_{n-1}} \sum_{\lambda_1=0}^{\lambda_2} G_1(\lambda_1)G_2(\lambda_2 - \lambda_1) \dots \dots \dots G_n(\lambda - \lambda_{n-1})$$

- T_8 : If $f(t) = (1 + t)^m$ then $F(\lambda) = \frac{m(m-1) \dots \dots (m-\lambda+1)}{\lambda!}$
- T_9 : If $f(t) = \sin(\omega t + \alpha)$ then $F(\lambda) = \frac{\omega^\lambda}{\lambda!} \sin\left(\frac{\pi\lambda}{2} + \alpha\right)$
- T_{10} : If $f(t) = \cos(\omega t + \alpha)$ then $F(\lambda) = \frac{\omega^\lambda}{\lambda!} \cos\left(\frac{\pi\lambda}{2} + \alpha\right)$

Application of DTM

Initially, we will transform Eqs. (11) and (12) under the above-mentioned theorem. Then we get the following iterative equations:

$$\begin{aligned}
 &(1 + R)(k + 4)(k + 3)(k + 2)(k + 1)F(k + 4) \\
 &+ R_o \left(\sum_{l=0}^k (l + 3)(l + 2)(l + 1)F(l + 3)F(k - l) \right) \\
 &- R((k + 2)(k + 1)G(k + 2)) + R_o M_n^2 (k + 2)(k + 1)F(k + 2) = 0 \tag{20}
 \end{aligned}$$

$$\begin{aligned}
 &\alpha(k + 2)(k + 1)G(k + 2) \\
 &- \beta R_o \left(\frac{1}{2} \sum_{l=0}^k (l + 1)F(l + 1)G(k - l) - \sum_{l=0}^k F(l)(k - l + 1)G(k - l + 1) \right) \\
 &+ R\{(k + 2)(k + 1)F(k + 2) - 2G(k)\} = 0 \tag{21}
 \end{aligned}$$

The transformed boundary conditions are as follows:

$$\begin{aligned}
 &F(0) = 0, F(1) = a, F(2) = 0, \\
 &F(3) = b, G(0) = 0, G(1) = c. \tag{22}
 \end{aligned}$$

where a, b, c can be evaluated by using appropriate boundary conditions mentioned in Eq. (16). We will get the approximate solution of $f(\eta)$ and $g(\eta)$ by using iteration from Eqs. (20) and (21).

Results and Discussion

In this division, the author highlights the impact of the different physical factors on the radial velocity $f'(\eta)$, the axial velocity $f(\eta)$ and the microrotation profile $g(\eta)$. For the validation of the differential transform method, the author presented comparative data of the outcomes achieved by DTM with the outcomes evaluated by the numerical method as well as results available in previous studies. This comparison is tabulated in Tables 1, 2 and 3.

In the Fig. 2, $f'(\eta)$ is discussed for various numeric values of magnetic field parameter M_n , by assigning other variables as a fixed value like micropolar variables $\alpha = 1, \beta = 0.001$ micropolar parameter $R = 1$ and the Reynolds number $R_o = 1$. The figure shows the

Table 1 Comparison between DTM and NM results, when $\alpha = 1, \beta = 0.001, R = 1, R_o = 1, M_n = 2$

η	f'		f		$-g$	
	DTM	NM	DTM	NM	DTM	NM
0.1	1.565464	1.565714	0.157906	0.157932	0.047141	0.047184
0.2	1.504863	1.505080	0.311752	0.311801	0.091159	0.091243
0.8	0.475429	0.475154	0.952253	0.952299	0.129602	0.129824
0.9	0.239237	0.238963	0.988036	0.988053	0.075901	0.076070

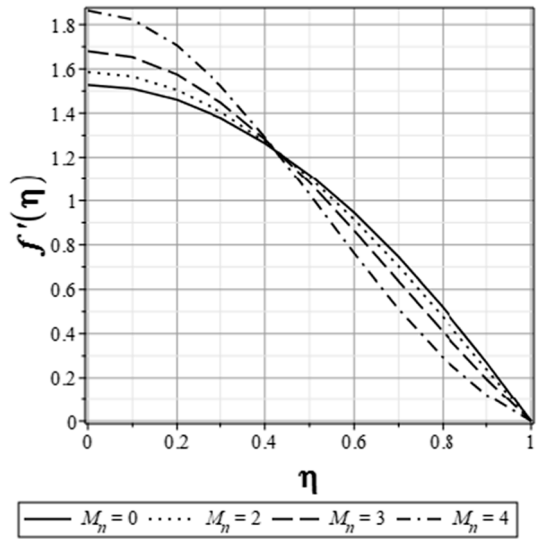
Table 2 Values of coefficient of skin friction ($-f''(1)$), when $\alpha = 1, \beta = 0.001, M_n = 1$

R_0	$R = 1$			$R = 3$			$R = 5$		
	DTM	NM	[23]	DTM	NM	[23]	DTM	NM	[23]
5	2.452397	2.452493	2.46753	2.414631	2.414732	2.45980	2.307222	2.307223	2.38259
3	2.634048	2.634065	2.60850	2.591021	2.591041	2.54472	2.432597	2.432655	2.44098
1	2.798887	2.798941	2.79806	2.691098	2.691113	2.64436	2.569310	2.569416	2.50649
0	2.714874	2.714908	2.71491	2.700153	2.700265	2.70026	2.542006	2.542101	2.54210
-1	3.053653	3.053718	3.04853	2.715444	2.715544	2.76052	2.567549	2.567669	2.57972
-3	3.399021	3.399077	3.37178	2.864397	2.864468	2.89495	2.677325	2.677467	2.66126
-5	3.730074	3.730184	3.77749	3.037555	3.037573	3.04929	2.748653	2.748759	2.75169

Table 3 Values of coefficient of couple stress ($g^*(1)$), when $\alpha = 1$, $\beta = 0.001$, $M_n = 1$

R_o	$R = 1$				$R = 3$				$R = 5$			
	DTM		NM		DTM		NM		DTM		NM	
	[23]	[23]	[23]	[23]	[23]	[23]	[23]	[23]	[23]	[23]	[23]	[23]
10	0.856587	0.856621	0.87129	0.87129	2.088053	2.088053	2.088075	2.088075	2.14447	2.14447	2.996555	2.996645
5	0.869186	0.869194	0.87736	0.87736	2.140187	2.140187	2.140298	2.140298	2.16929	2.16929	3.078236	3.078315
3	0.875635	0.875643	0.88060	0.88060	2.163608	2.163608	2.163619	2.163619	2.18102	2.18102	3.113309	3.113451
1	0.882663	0.882779	0.88442	0.88442	2.188082	2.188082	2.188097	2.188097	2.19386	2.19386	3.149764	3.149810
0	0.886444	0.886544	0.88654	0.88654	2.200656	2.200656	2.200706	2.200706	2.20071	2.20071	3.168333	3.168403

Fig. 2 Radial velocity graph for different M_n



decreasing behavior of the radial velocity from the lower to the upper disk. In addition, the radial velocity is increasing with a rise in the value of M_n up to approximately the middle of both the disks and decreases with a rise in the numeric value of M_n thereafter. The reason behind is that, on increasing the magnetic field parameter, Lorentz force increases automatically which create resistive force within the fluid, hence velocity decreases near the upper disk. In Fig. 3, the effect of M_n on $f(\eta)$ is displayed on the same above-mentioned fixed values. This figure illustrates that $f(\eta)$ is increasing throughout the gap length. One more observation can be seen from this figure which is, that the axial velocity has an increasing behavior with a rise in the values of M_n in the entire gap length. Figure 4 elucidates the

Fig. 3 Axial velocity graph for different M_n

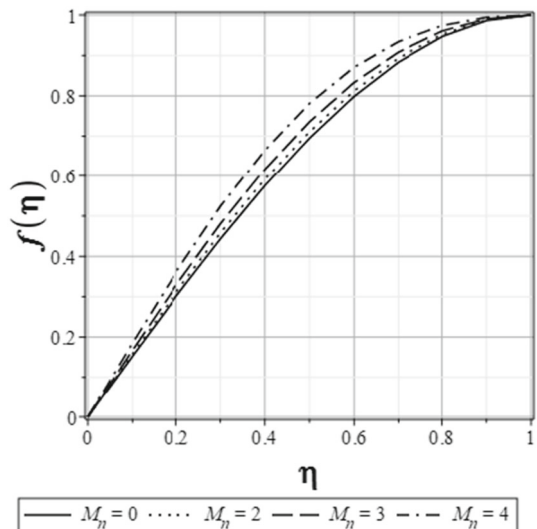
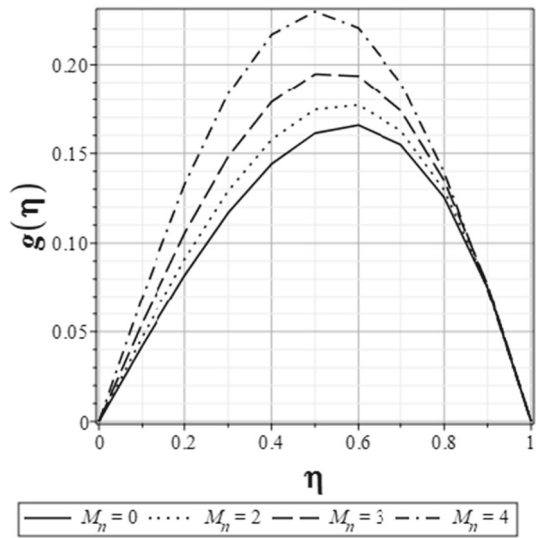


Fig. 4 Microrotation graph for different M_n



variation of the microrotation $g(\eta)$ for various values of M_n for the same fixed parameters. One observation can be made that the behavior of the microrotation is very close to the normal graph. In addition, increasing the value of M_n , it has an increasing behavior. The results of Figs. 3 and 4 are in the good agreement with the physical reason due to the applied magnetic field in the transverse direction which promotes both the velocity and the microrotation profiles.

Figures 5, 6 and 7 displays the variation of both profiles for distinct values of the micropolar parameters R after keeping other variables as constant like micropolar variables $\alpha = 1$, $\beta = 0.001$, micropolar parameter $R = 1$, the magnetic field parameter $M_n = 3$, the Reynolds

Fig. 5 Radial velocity graph for different R when $R_o = -1$

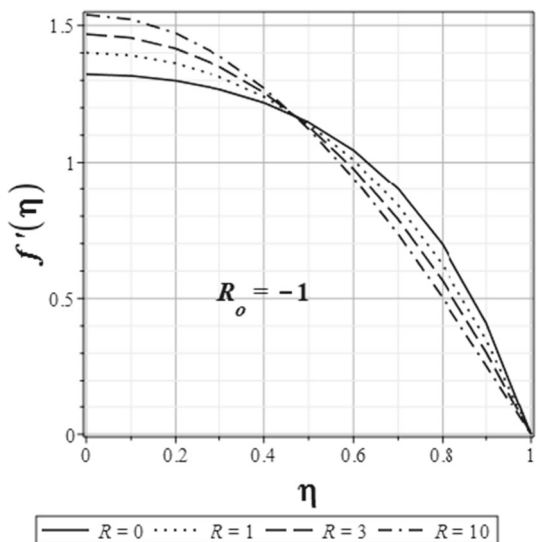


Fig. 6 Axial velocity graph for different R when $R_o = -1$

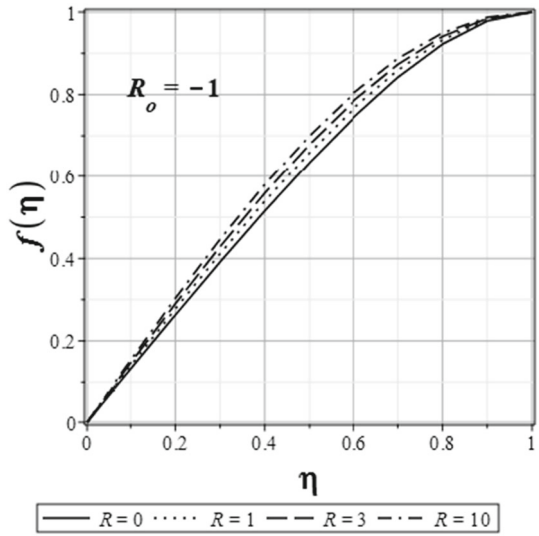
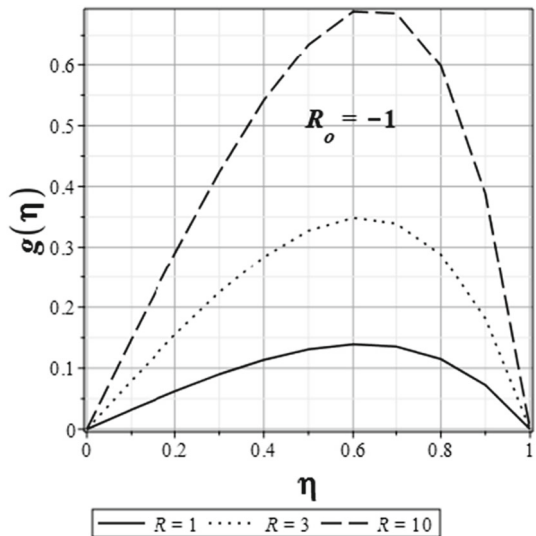


Fig. 7 Microrotation graph for different R when $R_o = -1$



number $R_o = -1$. We can observe from Fig. 5 that the radial velocity is falling continuously from $\eta = 0$ to $\eta = 1$. One more thing can be observed that the radial velocity profile is increasing from the lower disk to the approximately middle of both the disks as we increase the value of R but as the velocity crosses its middle its behavior is reversed. The variation of $f(\eta)$ is reflected in Fig. 6. A continuous increasing behavior of velocity can be seen from $\eta = 0$ to $\eta = 1$. In addition, the axial velocity also rises with a rise in the values of R in the entire gap. The nature of $g(\eta)$ can be seen in Fig. 7. As per the graph, $g(\eta)$ has incremental nature with an increase in the micropolar parameter. One more observation can be made that the peak of the graph is shifting towards the upper disk on increasing the values of R .

The variation of R when the Reynolds number is fixed at $R_o = 1$, on different profiles are reflected in Figs. 8, 9 and 10 when other variables are having a fixed value mentioned above. The falling behavior of the radial velocity is displayed in Fig. 8. It is also clear from figure that the radial velocity profile is decreasing with rise in R in the neighbourhood of the lower disk but it has reversing nature thereafter. Figure 9 presents the variation of $f(\eta)$ for various value of the micropolar parameter. As per this figure, the value of the velocity profile is rising rapidly from the lower boundary to the upper boundary. One more observation can be made that velocity is decreasing with rise in R in the entire gap. The nature of the microrotation profile is shown in Fig. 10. This figure explains that $g(\eta)$ increases rapidly up

Fig. 8 Radial velocity graph for different R when $R_o = -1$

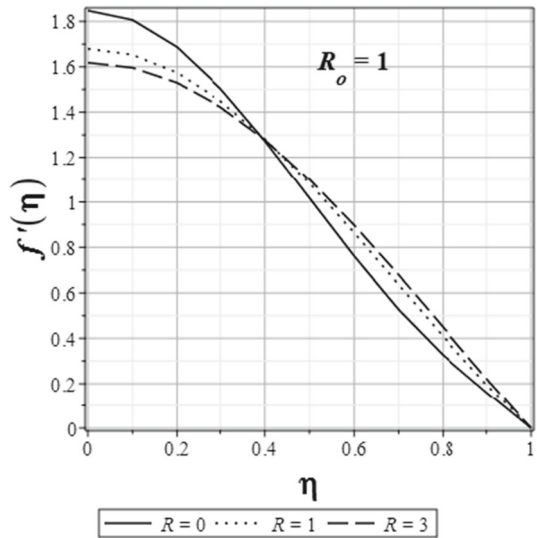


Fig. 9 Axial velocity graph for different R when $R_o = 1$

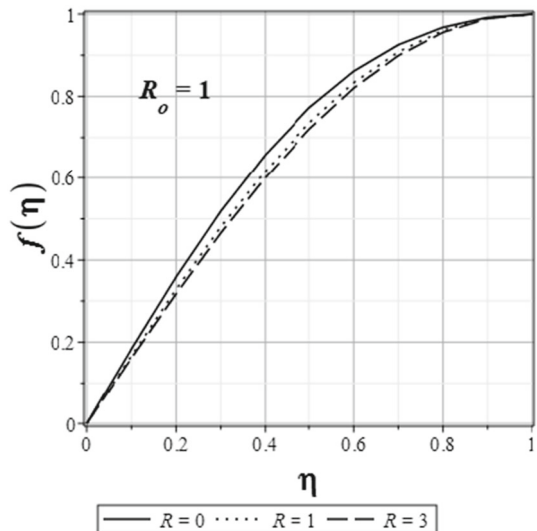
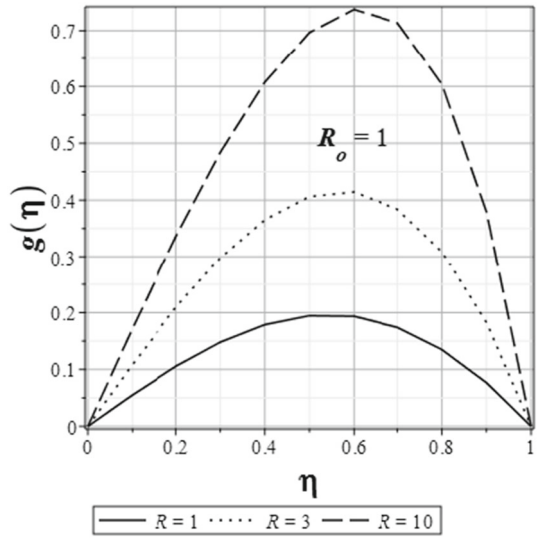


Fig. 10 Microrotation graph for different R when $R_o = 1$



to the approximate middle of the path and decreases up to the upper disk thereafter. It can also be analyzed that on rising the values of the micropolar parameter, the microrotation profile is also rising.

The impact of R_o on the radial, axial velocity and microrotation profile are displayed in Figs. 11, 12 and 13. The variation of the radial velocity $f'(\eta)$ is reflecting in Fig. 11 for various values of R_o by choosing other variables as a constant. This figure describes that the radial velocity is falling rapidly from $\eta = 0$ to $\eta = 1$. It can also be depicted that velocity is increasing with rising the values of R_o near the lower disk while decreasing with rising the values of R_o near the upper disk. The variation of the axial velocity $f(\eta)$ can be seen in

Fig. 11 Radial velocity graph for different R_o

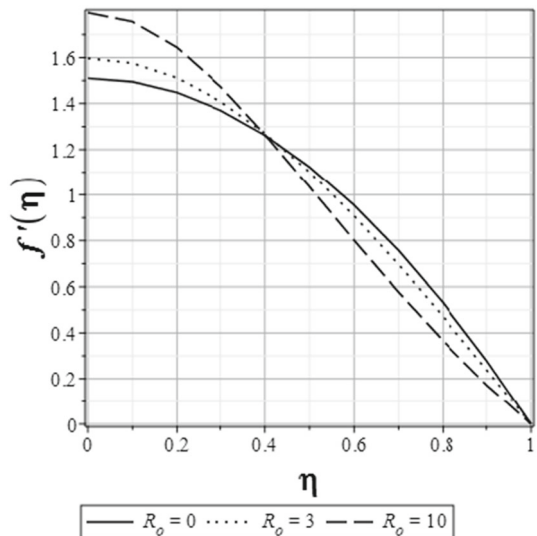


Fig. 12 Axial velocity graph for different R_o

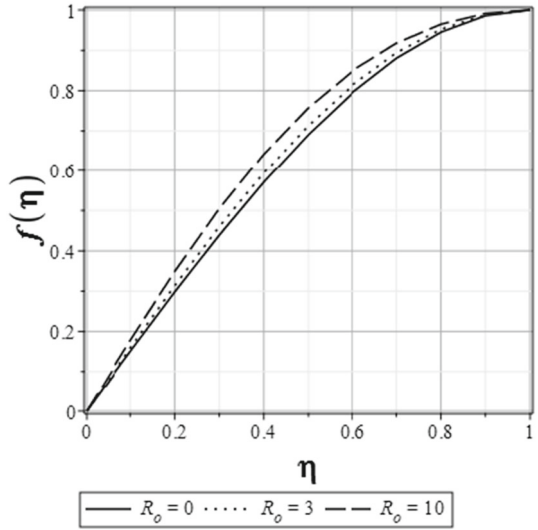


Fig. 13 Microrotation graph for different R_o

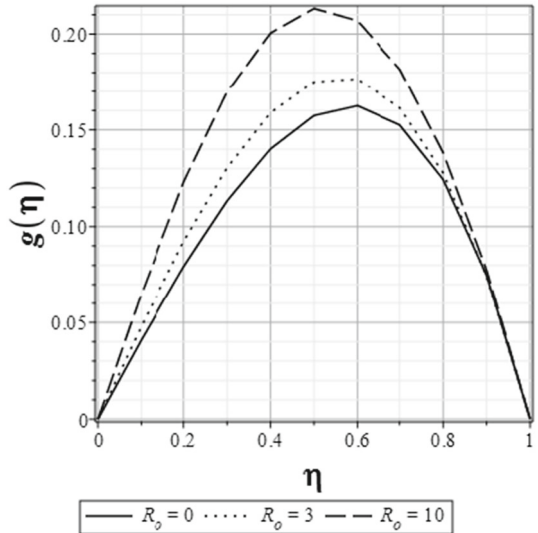


Fig. 12. This figure explaining the rising behavior of the axial velocity in the entire gap length as well as with respect to the distinct values of R_o . The variation of $g(\eta)$ for different values of R_o is presenting in Fig. 13. This graph describes the approximately normal behavior of the microrotation profile. It can also be depicted that the microrotation profile is increasing with rising the values of R_o .

Conclusion

The MHD flow of a micropolar fluid between two porous disks is discussed. The obtained higher-order nonlinear ODEs are evaluated by using DTM. The obtained outcomes are compared with the formerly available work which verifies the exactness and validity of the DTM. The author makes the following conclusions:

- The nature of the radial and the axial velocities are similar for the entire gap length. Its behavior is similar concerning the different parameters except for the distinct values of microrotation parameter while $R_o = 1$.
- The nature of the microrotation profile is very close to the normal graph from the lower to the upper disk. Also, it has an increasing behavior with respect to all physical parameters.
- The comparison of numeric values with literature shows that DTM is a better way for evaluating nonlinear ODEs.

In future study, we may generalize this model for the micropolar nanofluid with the effects of the magnetic fields.

Author contributions RG Conceptualization, methodology, software, validation, formal analysis, investigation, resources, data curation, writing original draft preparation, visualization, supervision.

Funding No funding.

Declarations

Conflict of interest The authors declare no Conflict of interest.

References

1. Eringen, A.C.: Simple microfluids. *Int. J. Eng. Sci.* **2**, 205–217 (1964). [https://doi.org/10.1016/0020-7225\(64\)90005-9](https://doi.org/10.1016/0020-7225(64)90005-9)
2. Eringen, A.C.: Theory of micropolar fluids. *J. Math. Mech.* **16**, 1–18 (1966)
3. Eringen, A. C.: *Microcontinuum field theories: I. Foundations and solids*. Springer Science and Business Media (2012)
4. Lukaszewicz, G. *Micropolar Fluids: Theory and applications*; Springer Science and Business Media, (1999)
5. Rashidi, M.M., Abelman, S., FreidooniMehri, N.: Entropy generation in steady MHD flow due to a rotating porous disk in a nanofluid. *Int. J. Heat Mass Transf.* **62**, 515–525 (2013). <https://doi.org/10.1016/j.ijheatmasstransfer.2013.03.004>
6. Mahanthesh, B., Gireesha, B.J., Shehzad, S.A., Rauf, A., Kumar, P.B.S.: Nonlinear radiated MHD flow of nanoliquids due to a rotating disk with irregular heat source and heat flux condition. *Phys. B Condens. Matter* **537**, 98–104 (2018). <https://doi.org/10.1016/j.physb.2018.02.009>
7. Soid, S.K., Ishak, A., Pop, I.: MHD flow and heat transfer over a radially stretching/shrinking disk. *Chin. J. Phys.* **56**, 58–66 (2018). <https://doi.org/10.1016/j.cjph.2017.11.022>
8. Aziz, A., Alsaedi, A., Muhammad, T., Hayat, T.: Numerical study for heat generation/absorption in flow of nanofluid by a rotating disk. *Results Phys.* **8**, 785–792 (2018). <https://doi.org/10.1016/j.rinp.2018.01.009>
9. Agarwal, R., Kumar Mishra, P.: Analytical solution of the MHD forced flow and heat transfer of a non-newtonian visco-inelastic fluid between two infinite rotating disks. *Mater. Today Proc.* **46**, 10153–10163 (2021). <https://doi.org/10.1016/j.matpr.2020.10.632>
10. Krishna, M.V., Chamkha, A.J.: Hall effects on MHD squeezing flow of a water-based nanofluid between two parallel disks. *J. Porous Media* (2019). <https://doi.org/10.1615/JPorMedia.2018028721>
11. Ibrahim, M.: Numerical analysis of time-dependent flow of viscous fluid due to a stretchable rotating disk with heat and mass transfer. *Results Phys.* **18**, 103242 (2020). <https://doi.org/10.1016/j.rinp.2020.103242>

12. Gupta, R.: Flow of a second-order fluid due to disk rotation. In: *Advances in Mathematical and Computational Modeling of Engineering Systems* (pp. 315–333). CRC Press (2023)
13. Turkyilmazoglu, M.: Fluid flow and heat transfer over a rotating and vertically moving disk. *Phys. Fluids* **30**, 063605 (2018). <https://doi.org/10.1063/1.5037460>
14. Agarwal, R.: Analytical study of micropolar fluid flow between two porous disks. *PalArchs J. Archaeol. Egypt Egyptol.* **17**, 903–924 (2020)
15. Venerus, D.C.: Squeeze flows in liquid films bound by porous disks. *J. Fluid Mech.* **855**, 860–881 (2018). <https://doi.org/10.1017/jfm.2018.635>
16. Waqas, H., Shehzad, S.A., Khan, S.U., Imran, M.: Novel numerical computations on flow of nanoparticles in porous rotating disk with multiple slip effects and microorganisms. *J. Nanofluids* **8**, 1423–1432 (2019). <https://doi.org/10.1166/jon.2019.1702>
17. Asma, M., Othman, W.A.M., Muhammad, T., Mallawi, F., Wong, B.R.: Numerical study for magnetohydrodynamic flow of nanofluid due to a rotating disk with binary chemical reaction and arrhenius activation energy. *Symmetry* **11**(10), 1282 (2019). <https://doi.org/10.3390/sym11101282>
18. Devaki, B., Pai, N.P., Vs SK: Analysis of MHD flow and heat transfer of casson fluid flow between porous disks. *J Adv Res Fluid Mech Therm Sci* **83**(1), 46–60 (2021)
19. Upadhya, S.M., Devi, R.L.V.R., Raju, C.S.K., Ali, H.M.: Magnetohydrodynamic nonlinear thermal convection nanofluid flow over a radiated porous rotating disk with internal heating. *J. Therm. Anal. Calorim.* **143**, 1973–1984 (2021). <https://doi.org/10.1007/s10973-020-09669-w>
20. Usman Lin, P., Ghaffari, A.: Steady flow and heat transfer of the power-law fluid between two stretchable rotating disks with non-uniform heat source/sink. *J Therm Anal Calorimet* **146**, 1735–1749 (2021)
21. Agarwal, R.: Heat and mass transfer in electrically conducting micropolar fluid flow between two stretchable disks. *Mater. Today Proc.* **46**, 10227–10238 (2021). <https://doi.org/10.1016/j.matpr.2020.11.614>
22. Doh, D.H., Muthamilselvan, M.: Thermophoretic particle deposition on magnetohydrodynamic flow of micropolar fluid due to a rotating disk. *Int. J. Mech. Sci.* **130**, 350–359 (2017). <https://doi.org/10.1016/j.ijmecsci.2017.06.029>
23. Takhar, H.S., Bhargava, R., Agrawal, R.S., Balaji, A.V.S.: Finite element solution of micropolar fluid flow and heat transfer between two porous discs. *Int. J. Eng. Sci.* **38**, 1907–1922 (2000). [https://doi.org/10.1016/S0020-7225\(00\)00019-7](https://doi.org/10.1016/S0020-7225(00)00019-7)
24. Sajid, M., Sadiq, M.N., Ali, N., Javed, T.: Numerical simulation for homann flow of a micropolar fluid on a spiraling disk. *Eur. J. Mech. BFluids* **72**, 320–327 (2018). <https://doi.org/10.1016/j.euromechflu.2018.06.008>
25. Lubrication Effects on Axisymmetric Flow of a Micropolar Fluid by a Spiraling Disk | SpringerLink Available online: <https://link.springer.com/article/https://doi.org/10.1007/s40430-020-02469-1> Accessed on 2 Sep 2023
26. Mohyud-Din, S.T., Jan, S.U., Khan, U., Ahmed, N.: MHD flow of radiative micropolar nanofluid in a porous channel: optimal and numerical solutions. *Neural Comput. Appl.* **29**, 793–801 (2018). <https://doi.org/10.1007/s00521-016-2493-3>
27. Bhat, A., Katagi, N.N.: Micropolar fluid flow between a non-porous disk and a porous disk with slip: keller-box solution. *Ain Shams Eng. J.* **11**, 149–159 (2020). <https://doi.org/10.1016/j.asej.2019.07.006>
28. Bhat, A., Katagi, N.N.: Magnetohydrodynamic flow of micropolar fluid and heat transfer between a porous and a non-porous disk. *Arch. Akad. BARU Artic.* **75**, 59–78 (2021)
29. Pasha, P., Mirzaei, S., Zarinfar, M.: Application of numerical methods in micropolar fluid flow and heat transfer in permeable plates. *Alex. Eng. J.* **61**, 2663–2672 (2022). <https://doi.org/10.1016/j.aej.2021.08.040>
30. Gupta, R.: Comparative study of micropolar fluid flow between two disks. *Harbin Gongye Daxue Xuebao J Harbin Inst Technol.* **54**, 61–76 (2022)
31. Ahmad, S., Ashraf, M., Ali, K.: Numerical simulation of viscous dissipation in a micropolar fluid flow through a porous medium. *J. Appl. Mech. Tech. Phys.* **60**, 996–1004 (2019). <https://doi.org/10.1134/S0021894419060038>
32. Sharma, K., Kumar, S., Vijay, N.: Insight into the motion of water-copper nanoparticles over a rotating disk moving upward/downward with viscous dissipation. *Int. J. Mod. Phys. B* **36**, 2250210 (2022). <https://doi.org/10.1142/S0217979222502101>
33. Kumar, S., Sharma, K.: Mathematical modeling of MHD flow and radiative heat transfer past a moving porous rotating disk with hall effect. *Multidiscip. Model. Mater. Struct.. Model. Mater. Struct.* **18**, 445–458 (2022). <https://doi.org/10.1108/MMMS-04-2022-0056>
34. Kumar, S., Sharma, K.: Impacts of stefan blowing on reiner-rivlin fluid flow over moving rotating disk with chemical reaction. *Arab. J. Sci. Eng.* **48**, 2737–2746 (2023). <https://doi.org/10.1007/s13369-022-07008-9>

35. Kumar, S., Sharma, K.: Darcy-forchheimer fluid flow over stretchable rotating disk moving upward/downward with heat source/sink. *Spec Top Rev Porous Med: Int J* (2022). <https://doi.org/10.1615/SpecialTopicsRevPorousMedia.2022043951>
36. Kumar, S., Sharma, K.: Entropy optimization analysis of marangoni convective flow over a rotating disk moving vertically with an inclined magnetic field and nonuniform heat source. *Heat Transf.* **52**, 1778–1805 (2023). <https://doi.org/10.1002/htj.22763>
37. Sharma, K., Kumar, S.: Impacts of low oscillating magnetic field on ferrofluid flow over upward/downward moving rotating disk with effects of nanoparticle diameter and nanolayer. *J. Magn. Magn. Mater. Magn. Mater.* **575**, 170720 (2023). <https://doi.org/10.1016/j.jmmm.2023.170720>
38. Kumar, S., Sharma, K., Makinde, O.D., Joshi, V.K., Saleem, S.: Entropy generation in water conveying nanoparticles flow over a vertically moving rotating surface: keller box analysis. *Int J Num Methods Heat Fluid Flow* (2023). <https://doi.org/10.1108/HFF-05-2023-0259>
39. Zhou, J.K.: Differential transformation and its applications for electrical circuits. In: Huazhong University Press, Wuhan, China (1986)
40. Usman, M., Hamid, M., Khan, U., Mohyud Din, S.T., Iqbal, M.A., Wang, W.: Differential transform method for unsteady nanofluid flow and heat transfer. *Alex. Eng. J.* **57**, 1867–1875 (2018). <https://doi.org/10.1016/j.aej.2017.03.052>
41. Keimanesh, M., Rashidi, M.M., Chamkha, A.J., Jafari, R.: Study of a third grade non-newtonian fluid flow between two parallel plates using the multi-step differential transform method. *Comput. Math. Appl.* **62**, 2871–2891 (2011). <https://doi.org/10.1016/j.camwa.2011.07.054>
42. Hatami, M., Jing, D.: Differential transformation method for newtonian and non-newtonian nanofluids flow analysis: compared to numerical solution. *Alex. Eng. J.* **55**, 731–739 (2016). <https://doi.org/10.1016/j.aej.2016.01.003>
43. Agarwal, R. Squeezing MHD: Flow along with heat transfer between parallel plates by using the differential transform method. *Стиснення MHD потоку разом із теплопередачею між паралельними пластинами за допомогою методу диференціального перетворення* (2022)
44. Gupta, R., Selvam, J., Vajravelu, A., Nagapan, S.: Analysis of a squeezing flow of a casson nanofluid between two parallel disks in the presence of a variable magnetic field. *Symmetry* **15**, 120 (2023). <https://doi.org/10.3390/sym15010120>
45. Balazadeh, N., Sheikholeslami, M., Ganji, D.D., Li, Z.: Semi analytical analysis for transient eyring-powell squeezing flow in a stretching channel due to magnetic field using DTM. *J. Mol. Liq.* **260**, 30–36 (2018). <https://doi.org/10.1016/j.molliq.2018.03.066>
46. Gupta, R., Agrawal, D.: Flow analysis of a micropolar nanofluid between two parallel disks in the presence of a magnetic field. *J. Nanofluids* **12**, 1320–1326 (2023). <https://doi.org/10.1166/jon.2023.2021>
47. Awati, V.B., Jyoti, M., Bujurke, N.M.: Series solution of steady viscous flow between two porous disks with stretching motion. *J. Nanofluids* **7**, 982–994 (2018). <https://doi.org/10.1166/jon.2018.1512>
48. Agarwal, R. An analytical study of non-newtonian visco-inelastic fluid flow between two stretchable rotating disks.
49. Gupta, R.: Homotopy perturbation method for the MHD second-order fluid flow through a channel with permeable sides. *Harbin Gongye Daxue Xuebao/Journal Harbin Inst Technol.* **54**, 38–45 (2022)
50. Ganji, D.D., Abbasi, M., Rahimi, J., Gholami, M., Rahimipetroudi, I.: On the MHD squeeze flow between two parallel disks with suction or injection via HAM and HPM. *Front. Mech. Eng.* **9**, 270–280 (2014). <https://doi.org/10.1007/s11465-014-0303-0>

Publisher's Note Springer Nature remains neutral with regard to jurisdictional claims in published maps and institutional affiliations.

Springer Nature or its licensor (e.g. a society or other partner) holds exclusive rights to this article under a publishing agreement with the author(s) or other rightsholder(s); author self-archiving of the accepted manuscript version of this article is solely governed by the terms of such publishing agreement and applicable law.